Title: **Practical Development of HMD and Application to High-rise Buildings**

Authors: Hirofumi Okuda, Deputy Manager, Obayashi Corporation
Mitsuru Kageyama, Deputy General Manager, Obayashi Corporation
Masayuki Yamanaka, Group Leader, Obayashi Corporation
Matsutaro Seki, General Manager, Obayashi Corporation

Subject: Structural Engineering

Keywords: Tuned Mass Damper
Vibrations

Publication Date: 2004

Original Publication: CTBUH 2004 Seoul Conference

Paper Type:
1. Book chapter/Part chapter
2. Journal paper
3. **Conference proceeding**
4. Unpublished conference paper
5. Magazine article
6. Unpublished

Practical Development of HMD and Application to High-rise Buildings

Hirofumi Okuda[1], Mitsuru Kageyama[2], Masayuki Yamanaka[3], Matsutaro Seki[4]

[1] Deputy Manager, Technical Research Institute, Obayashi Corporation
[2] Deputy General Manager, Technical Research Institute, Obayashi Corporation
[3] Group Leader, Design Department, Obayashi Corporation
[4] General Manager, Technical Research Institute, Obayashi Corporation

Abstract

This paper describes development of a Hybrid Mass Damper (HMD) and its application to four actual high-rise buildings. This HMD consists of an Active Mass Damper (AMD) installed on a Tuned Mass Damper (TMD) supported by four Multi-Layer Laminated Rubber Bearings. This HMD has a merit which makes it possible to shift smoothly from TMD to HMD according to the response level of building. The applied active control systems have a merit to make it possible to control the multi modes including torsional modes of building. This paper presents the solutions of those problems, and shows the vibration control effects.

Keywords: hybrid mass damper; variable gain control; stroke constraint; velocity constraint; optimum filter

1. Introduction

For the purpose of improving the vibration amenity of high-rise building under strong winds or small-to-medium earthquakes, authors have been developing the active vibration control method that is composed of AC servomotor and ball screw shaft[1-5]. We have developed two types. One is AMD which is full active type, and the other is HMD which has the AMD on passive type TMD composed of added mass (namely passive mass) and Multi-Layer Laminated Rubber Bearing. This paper describes mainly the methods to construct HMD.

In advance of the actual use of above-mentioned equipment, it was necessary to solve three important subjects as follows: how to correct the non-linear stiffness of Multi-Layer Laminated Rubber Bearing used in HMD, how to avoid the control-spillover, and how to control the stroke and velocity of AMD within its limitation in the case that large external force out of consideration acts on building. This paper presents the methods to cope with the above-mentioned three subjects, the buildings in which HMD is installed and the vibration control effects.

2. Outlines of Building and Device

The active vibration control device is installed in a building that is shown in Fig.1. This HMD is installed in a building of DENTSU INC. New Head Office in 2002. The Dentsu tower has a unique shape of the floor plan which looks like crescent or boomerang. The frames spanning 15.9m are set at 7.2m intervals along about 140m long crescent shape and create boomerang shape office floor on the south side and service space inside. At the north side, rigid frames around the shuttle elevators are connected to the boomerang frames by two-story high reverse V-braces at the five floors where the shuttle elevators serve.

Contact Author : Hirofumi Okuda
Deputy Manager
Technical Research Institute, Obayashi Corporation
4-640, Shimokiyoto, Kiyose-shi, Tokyo, JAPAN
Tel: +81-424-95-0944 Fax: +81-424-95-0904
e-mail: okuda.hirofumi@obayashi.co.jp

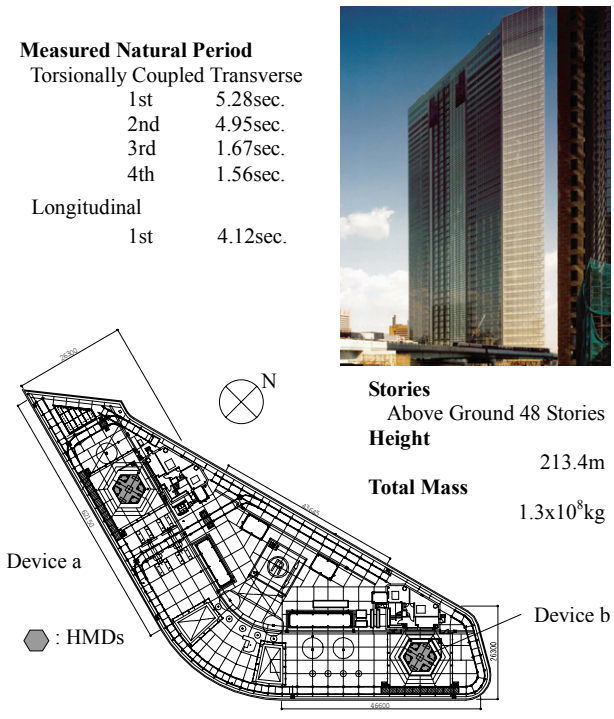

Fig. 1. Installed Building and the Location of Setting Devices

The outline of the composition of HMD is shown in Fig.2. The HMD consists of the AMD installed on the TMD which is supported with four Multi-Layer Laminated Rubber Bearing systems, two tensile spring systems and four compressive spring systems. The compressive spring works for correcting non-linear stiffness of Multi-Layer Laminated Rubber Bearings. The details are given in chapter 4. The passive part of HMD is equipped with anti-twist mechanism composed of linear bearing and the braking system that works under large external force such as large earthquakes. The HMD system acts as TMD in the right-angled direction, because the Multi-Layer Laminated Rubber Bearing in the HMD has the coil springs between the element of rubber bearings in the right-angled direction to the active one for tuning the period of its direction.

Fig.3 shows the results of comparing between the measured responses and ones derived from analyzing with reduction model.

3. Identification of AMD and its Converting Method

It is difficult to develop the characteristic of AC servomotor theoretically, because AC servomotor is driven with the three-phased electric current. Therefore we decided to make the device model from the observed characteristic of AMD. Original AC servomotor has characteristic with the velocity controlled type, and its characteristic is expressed as follows:

$$\frac{\dot{z}}{v} = \frac{\beta}{s^2 + \alpha_1 s + \alpha_0} \tag{1}$$

where, α_0 , α_1 and β mean the coefficients of dynamic characteristic of AC servomotor, v means input voltage to AC servomotor, z means the stroke displacement of active mass of AMD, and s means the variable of Laplace transformation.

It was difficult to control directly the stroke of AMD within its limits under the large input force, because the conventional AC servomotor has characteristic with velocity controlled type[1-3]. Authors hence developed the method of converting the characteristic of AC servomotor from its original velocity controlled type into displacement controlled type with installing minor loops for AC servomotor[4-5]. We decide to introduce the minor loop gains for above-mentioned purpose, and they are found under the condition that the acceleration feed back gain of AMD is not used because of escaping the control-spillover caused by acceleration feed-back loop. Fig.4 shows the concept of block diagram that has minor loops with displacement and velocity gains of the AC servomotor. The characteristic of transfer function from v to $\dot{z}$ in Fig.4 is expressed in equation (1).

Mass	AMD:2.0x10^{4}kg , TMD:2.0x10^{5}kg
Maximum Stroke	AMD:105.0cm , TMD:70.0cm
Maximum Force	26.1kN(AMD)
AC Servomotor	55kW(AMD)

The minor loop gains $G(g_d, g_v)$ is led with the aim

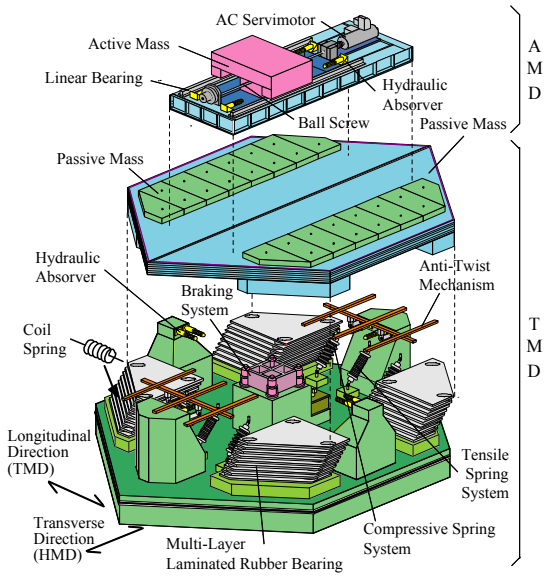

Fig. 2. Schematic and Specification of HMD

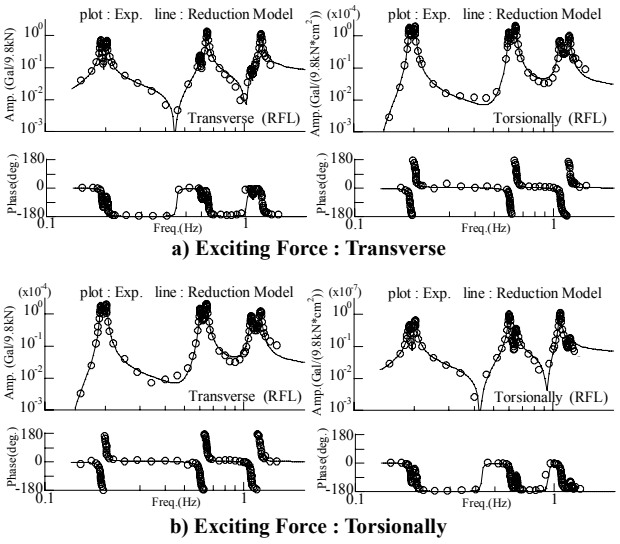

Fig. 3. Comparison between Measured and Calculated Responses from Reduction Model

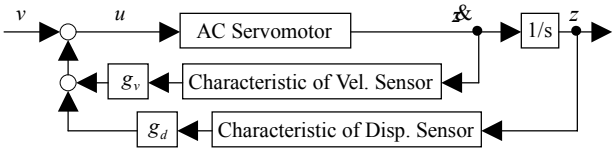

Fig. 4. Concept of the Minor Loops for AC Servomotor

of converting the transfer function from u to z into the constant in its low frequency, namely, displacement controlled type. Input voltage v to the motor is expressed in equation (2) by using the manipulated voltage u and the voltage from the minor loops. Incidentally, equation (2) contains a sensor characteristic.

$$v = u - \left(\frac{b}{s^2 + a_1 s + a_0} g_d + \frac{d}{s^2 + c_1 s + c_0} g_v s \right) z \qquad (2)$$

where, a_1 , a_0 and b mean the coefficients of dynamic characteristic of displacement sensor, c_1 , c_2 and d mean the coefficients of dynamic characteristic of velocity sensor. Equation (3) is derived from substituting equation (2) for (1) using relationship $\dot{x} = sz$.

$$\frac{x_a}{u} = \frac{\beta(s^4 + Hs^3 + Is^2 + Js + K)}{s^7 + As^6 + Bs^5 + Cs^4 + Ds^3 + Es^2 + Fs + G} \qquad (3)$$

$$A = \alpha_1 + H \ , \quad B = \alpha_0 + \alpha_1 H + I \ , \quad C = \alpha_0 H + \alpha_1 I + J \ ,$$
$$D = \alpha_0 I + \alpha_1 J + K + \beta d_0 g_v \ , \quad E = \alpha_0 J + \alpha_1 K + \beta(b g_d + a_1 d g_1) \ ,$$
$$F = \alpha_0 K + \beta(b c_1 g_d + a_0 d g_1) \ , \quad G = \beta b c_0 g_d \ , \quad H = a_1 + c_1 \ ,$$
$$I = a_0 + c_0 + a_1 c \ , \quad J = a_0 c_1 + a_1 c_0 \ , \quad K = a_0 c_0$$

A characteristic change of AC servomotor is shown in the following way. In other words, by using a minor loops, a low mode area of the building is made a displacement controlled type and then a high mode area is made a velocity controlled type. Here, a minor loop gains $G(g_d, g_v)$ is fixed by the following expression.

$$\begin{matrix} z/u \\ sz/u \end{matrix} \Big\rangle \ s = i\omega \ \Rightarrow \ \left\langle \begin{matrix} D(\omega) & \xrightarrow[\text{(differential)}]{} & D'(\omega) & \xrightarrow[\text{(1st, 2nd Mode)}]{\text{Torsionally Coupled Transverse}} & 0 \\ V(\omega) & \xrightarrow[\text{(differential)}]{} & V'(\omega) & \xrightarrow[\text{(3rd, 4th Mode)}]{} & 0 \end{matrix} \right.$$

Fig. 5 shows a converted and conventional characteristics which is actually installed on DENTSU INC. New Head Office. In the case of using AC servomotor with above mentioned minor loops, it has the effect to prevent the displacement and velocity of active mass from overshooting to input signal.

4. Composition if HMD and Correcting Method of Non-linearity

Our proposed HMD is composed of above AMD set on passive mass of TMD supported with Multi-Layer Laminated Rubber Bearing. The Multi-Layer Laminated Rubber Bearing has no friction drag, thus TMD has the merit to move smoothly from small external force level. It becomes possible to shift the proposed device smoothly from TMD to HMD according to the response level of building. However, the passive mass system works as TMD only in the case that the response amplitude is within the limited range. Because in the case of DENTSU INC. New Head Office, though this building itself has almost the linear characteristic as shown in Fig.6, the Multi-Layer Laminated Rubber Bearing constructing TMD has non-linear characteristic of stiffness whose ratio of the restoring force to the deformation becomes smaller with the progress of its deformation. This figure also shows the characteristic of Multi-Layer Laminated Rubber Bearing actually used at DENTSU INC. New Head Office.

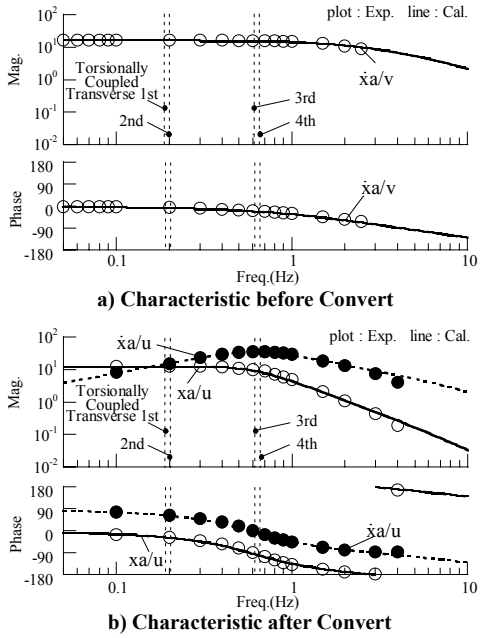

Fig. 5. Transfer Function of AMD (Device a)

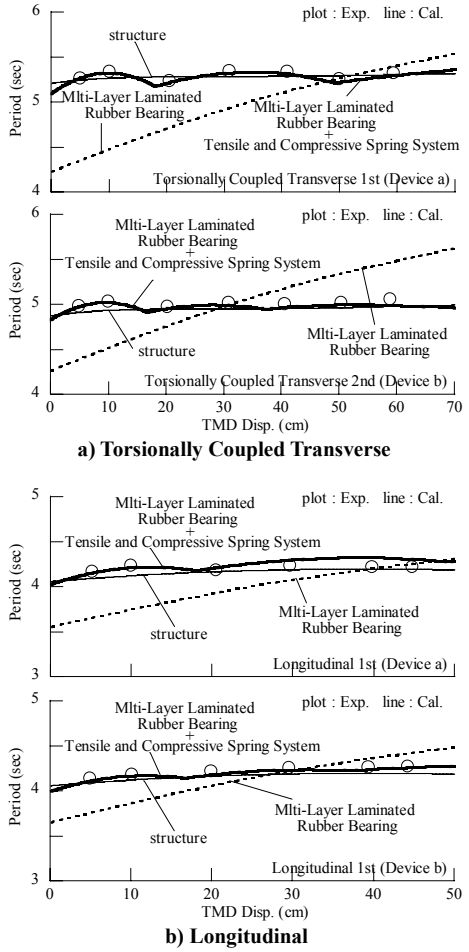

Fig. 6. Correcting Method of Non-linearity of Multi-Layer Laminated Rubber Bearing

Therefore we developed the method to correct the non-linear characteristic of TMD composed of Multi-Layer Laminated Rubber Bearing. Our proposed method is shown in Fig.7 that is composed

of the compressive spring installed between passive mass and installed floor of building with pin-supports at the both edges. In comparing the characteristic of Multi-Layer Laminated Rubber Bearing with the target characteristic as shown in Fig.6, Multi-Layer Laminated Rubber Bearing has too large restoring force comparing with the target one as far as they intersect. On the other hand, the compressive spring system generates negative restoring force in the range where the compression exists. This compressive spring system does not generate positive restoring force because the spring part leaves the pin-support part in the range where the tension works in the spring. The characteristic of compressive spring system is shown in Fig.6.

The compressive spring gives the passive mass the horizontal component force P_x which is expressed as follows:

$$P_x = -k\left(L_0 - \sqrt{x_P^2 + H^2} \right)\sin\theta \tag{4}$$

where H, x_P, L_0, k denote the vertical length between the both edges of pin-support, the relative displacement of passive mass to its basement, natural length of the spring without stress, and stiffness of the spring respectively. And θ represents the angle of displacement x_P to vertical length H as shown in Fig.7, thus $\sin\theta$ is represented as follows:

$$\sin\theta = x_P \Big/ \sqrt{x_P^2 + H^2} \tag{5}$$

Equation (4) is rewritten by substituting equation (5) for (4) as follows:

$$P_x = -\frac{k\, x_P (L_0 - \sqrt{x_P^2 + H^2})}{\sqrt{x_P^2 + H^2}} \tag{6}$$

We conduct the differential calculus of equation (6) to x_P for the purpose of knowing the position where equation (6) has the maximum.

$$\frac{\partial P_x}{\partial x_P} = \frac{k\{(x_P^2 + H^2)^{3/2} - L_0 H^2\}}{(x_P^2 + H^2)^{3/2}} \tag{7}$$

The condition for equation (6) having the maximum is given as follows:

$$H^4 L_0^2 = (x_M^2 + H^2)^3 \tag{8}$$

where x_M denotes the displacement at which equation (6) has the maximum. When defining x_0 as the passive mass displacement at which the restoring force of the Multi-Layer Laminated Rubber Bearing agrees with that of the target, x_0 must meet the following condition.

$$L_0^2 = x_0^2 + H^2 \tag{9}$$

By solving the simultaneous equation of equation (8) and (9), H which satisfies the condition of specified x_M and x_0 is given as follows:

$$H = \left\{ \frac{x_M^3 (3x_M + \sqrt{4x_0^2 - 3x_M^2})}{2(x_0^2 - 3x_M^2)} \right\}^{1/2} \tag{10}$$

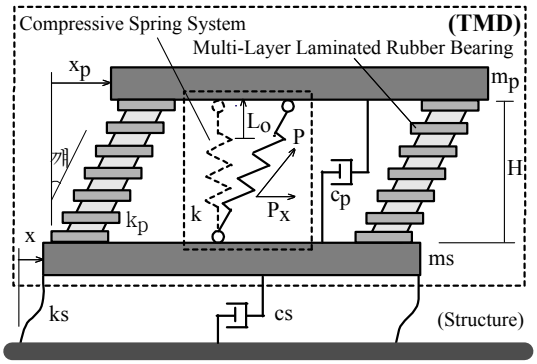

Fig. 7. Concept of the Compressive Spring System for Non-linear Characteristic

It is found that x_M becomes smaller than $1/\sqrt{3}$ of x_0 as shown in equation (11), because the denominator of equation (10) must be positive.

$$x_M \text{값} x_0 / \sqrt{3} \tag{11}$$

The natural length of the spring L_0 is derived from equation (9) as follows:

$$L_0 = \sqrt{x_0^2 + H^2} \tag{12}$$

We adjust x_M to the position of the maximum difference between restoring force of the target and Multi-Layer Laminated Rubber Bearing. In denoting the maximum difference of both restoring forces as P_M, and in substituting P_M and x_M for P_x and x_P in equation (6), the optimum stiffness of the compressed spring k is given as follows:

$$k = \frac{P_M \sqrt{x_M^2 + H^2}}{x_M (L_0 - \sqrt{x_M^2 + H^2})} \tag{13}$$

We introduce the 2nd compressed spring to complement of the range of displacement position where non-linearity can not be corrected only by the 1st one. The 1st system mainly corrects the characteristic in the range of large x_P, and the 2nd system corrects that in the range of small x_P.

Fig.6 shows the actual case using the method that adjusts the characteristic of TMD.

5. Formulation on State Equation

The block diagram of the whole control system is shown in Fig.8. The state equation of the AC servomotor characteristic of the device a which is converted with minor loops in Chapter 2 is shown as follows:

$$\dot{Z}_a = A_{za} Z_a + B_{za} u_{za} \tag{14}$$

When the device b is defined in same way, the expanded state equation joining both devices is shown as follows:

$$\dot{Z}_g = A_{zg} Z_g + B_{zg} U_{zg} \tag{15}$$

$$Z_g{}^T = ((z_a \quad \dot{z}_a \quad \ddot{z}_a)(z_b \quad \dot{z}_b \quad \ddot{z}_b)),$$

$$A_{zg} = \begin{bmatrix} A_{za} & [0] \\ [0] & A_{zb} \end{bmatrix}, \quad B_{zg} = \begin{bmatrix} B_{za} & \{0\} \\ \{0\} & B_{zb} \end{bmatrix}, \quad U_{zg}{}^T = (u_{za} \quad u_{zb})$$

An expanded equation combining equation (15) and the building characteristic to have included TMD characteristic is represented as follows:

$$\dot{\overline{X}} = A\overline{X} + BU_{zg} \tag{16}$$

$$\overline{X}^T = (\overline{X}_S{}^T \quad Z_g{}^T), \quad A = \begin{bmatrix} A_S & B_S C_z \\ [0] & A_{zg} \end{bmatrix},$$

$$B = \begin{Bmatrix} [0] \\ B_{zg} \end{Bmatrix}, \quad C_Z = \begin{bmatrix} 0 & 0 & 1 & 0 & 0 & 0 \\ 0 & 0 & 0 & 0 & 0 & 1 \end{bmatrix}$$

As the filter system is necessary to avoid the control-spillover caused by ignored high modes, the filter system is added to above system in equation (16). When u_{za} denotes the input signal to device a in equation (16), the signal u_{za} is defined as output signal from filter a whose characteristic is represented in equation (17).

$$\dot{X}_{fa} = A_{fa}X_{fa} + B_{fa}u_{sa}, \quad u_{za} = C_{fa}X_{fa} \tag{17}$$

The filter to device b is similarly shown as follows:

$$\dot{X}_{fb} = A_{fb}X_{fb} + B_{fb}u_{sb}, \quad u_{zb} = C_{fb}X_{fb} \tag{18}$$

The expanded state equation joining above both original filter systems is shown as follows:

$$\dot{X}_f = A_f X_f + B_f U_f, \quad U_{zg} = C_f X_f \tag{19}$$

$$X_f{}^T = (X_{fa}{}^T \quad X_{fb}{}^T), \quad U_f{}^T = (u_{sa} \quad u_{sa}), \quad Y_f{}^T = (u_{za} \quad u_{zb}),$$

$$A_f = \begin{bmatrix} A_{fa} & [0] \\ [0] & A_{fb} \end{bmatrix}, \quad B_f = \begin{bmatrix} B_{fa} & \{0\} \\ \{0\} & B_{fb} \end{bmatrix}, \quad C_f = \begin{bmatrix} C_{fa} & (0) \\ (0) & C_{fb} \end{bmatrix}$$

The expanded equation combining equations (16) and (19) is expressed as follows:

$$\dot{X}_G = A_G X_G + B_G U_G \tag{20}$$

$$X_G{}^T = (X_S{}^T \quad Z^T \quad X_f{}^T), \quad A_G = \begin{bmatrix} A & BC_f \\ [0] & A_f \end{bmatrix}, \quad B_G = \begin{bmatrix} [0] \\ B_f \end{bmatrix}$$

6. Formation of the Optimum Filter

Equation (21) denotes the feedback gain vectors that are calculated by applying the optimum control theory to equation (20) under the condition that the control weightings are given to the velocity responses of the building and the displacements of passive masses.

$$\overline{K} = [\,\overline{K}_S \quad \overline{K}_Z \quad \overline{K}_f\,] \tag{21}$$

The operating value U_G of equation (20) can be rewritten into equation (22) that is divided into the gains for the filter and the others.

$$U_G = -[[0] \quad [0] \quad \overline{K}_f]X_G - [\,\overline{K}_S \quad \overline{K}_Z \quad [0]\,]X_G \tag{22}$$

When replacing the secondary term of equation (22) with U_R, and shifting the first term of it into A_G of equation (20), in this case, equation (20) is rewritten as follows:

$$\dot{X}_G = A_{Gf}X_G + B_G U_R \tag{23}$$

$$A_{Gf} = \begin{bmatrix} A & BC_f \\ [0] & A_f - B_f\overline{K}_f \end{bmatrix},$$

$$U_R = -[\overline{K}_S \quad \overline{K}_Z \quad [0]]X_G = -[\overline{K}_S \quad \overline{K}_Z]\overline{X}$$

Because U_R denotes the input signal to filter system, it has the following condition:

$$U_R = U_f \tag{24}$$

Equation (23) expresses that A_f in equation (20) changes to $A_{f(opt)}$ in equation (25) where the optimum feed back gains are considered. Thus equation (25) gives the optimum filter.

$$A_{f(opt)} = A_f - B_f\overline{K}_f \tag{25}$$

The relationship of optimum filter between input signals and output signals are expressed as follows:

$$\dot{X}_f = A_{f(opt)}X_f + B_f\begin{Bmatrix} u_{sa} \\ u_{sb} \end{Bmatrix}, \quad \begin{Bmatrix} u_{za} \\ u_{zb} \end{Bmatrix} = C_f X_f \tag{26}$$

In the actual usage of above optimum filter system, equation (26) is replaced with digital filter in the

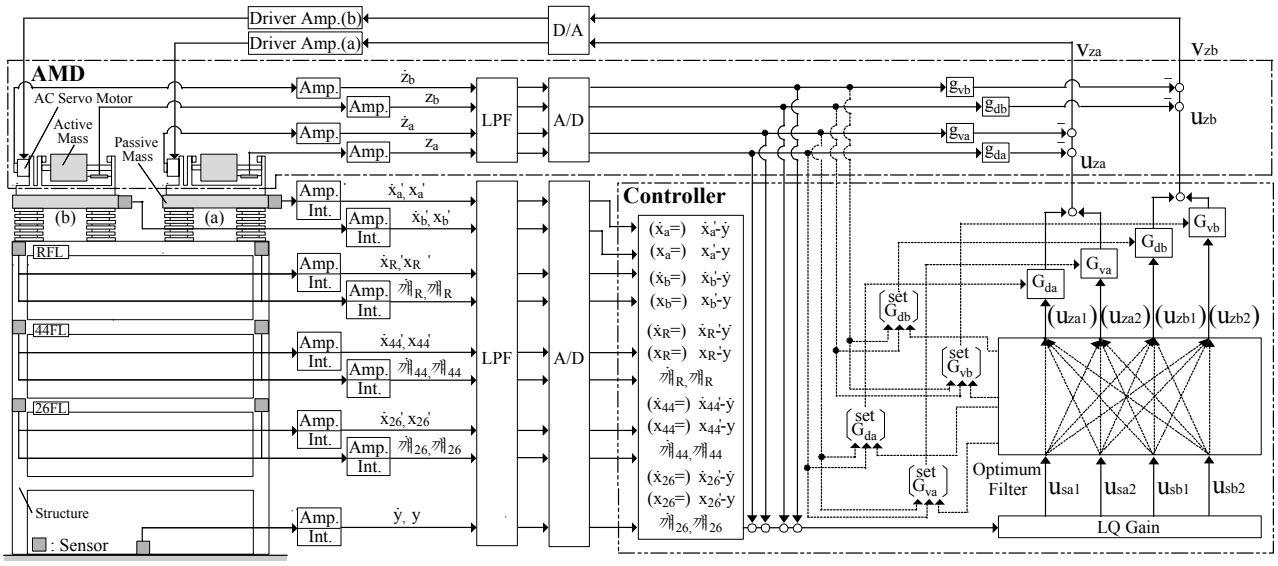

Fig. 8. Block Diagram of Control System

controller. The digital filtering method has a merit that makes it possible to calculate directly the output signal from input signal without calculating the responses of many state factors of filter system in the controller. Because digital filter is generally composed of the system with single input and single output, it has been difficult to apply the digital filter system to the above system that has four inputs and four outputs. Hence the above filter system is resolved into sixteen systems which have single input and single output. For example, the transfer function from u_{sa1} to u_{za1} is derived from using each corresponding component of B_{fa1} and C_{fa1} defined in equation (19) as follows:

$$W_{(za1/sa1)} = \left[C_{fa1} \quad (0) \quad (0) \quad (0)\right]\left[sI - A_{f(opt)}\right]^{-1}\begin{Bmatrix} B_{fa1} \\ \{0\} \\ \{0\} \\ \{0\} \end{Bmatrix} \tag{27}$$

From substituting the following bilinear transformation6 for s in the equation (27),

$$s = \frac{2}{T_d}\left(\frac{1 - z^{-1}}{1 + z^{-1}}\right) \tag{28}$$

where the symbol z and T_d denotes the variable of z-transform and sampling time respectively, and they are rewritten into the discrete-time system's functions. For example, the discrete transfer function from u_{sa1} to u_{za1} is represented as $H_{(za1/sa1)}$, which is derived from substituting equation (28) for s in equation (27). The output signal does not directly become to u_{za1}, because the signal u_{za1} is defined as the signal adding output signals from u_{sa} and u_{sb}. Hence it becomes necessary to have buffer $u'_{(za1/sa1)}$ before obtaining final output signals.

$$H_{(za1/sa1)} = \frac{u'_{(za1/sa1)}}{u_{sa1}} = \frac{b_1 z^{-1} + b_2 z^{-2} + \Lambda + b_{n_f} z^{-n_f}}{1 + a_1 z^{-1} + a_2 z^{-2} + \Lambda + a_{n_f} z^{-n_f}} \tag{29}$$

where n_f represents the number of the poles. Because z^{-1} means 1 step delay, $u'_{(za1/sa1)}$ in time domain is calculated as follows:

$$u'_{(za1/sa1)}(k) = \sum_{i=1}^{n_f} b_i * u_{sa1}(k-i) - \sum_{i=1}^{n_f} b_i * u'_{(za1/sa1)}(k-i) \tag{30}$$

Using the other components of buffers calculated in the same way, the final output signals from the filter system are calculated as follows:

$$u_{za1}(k) = u'_{(za1/sa1)}(k) + u'_{(za1/sa2)}(k) + u'_{(za1/sb1)}(k) + u'_{(za1/sb2)}(k) \tag{31}$$

$$u_{za2}(k) = u'_{(za2/sa1)}(k) + u'_{(za2/sa2)}(k) + u'_{(za2/sb1)}(k) + u'_{(za2/sb2)}(k) \tag{32}$$

$$u_{zb1}(k) = u'_{(zb1/sa1)}(k) + u'_{(zb1/sa2)}(k) + u'_{(zb1/sb1)}(k) + u'_{(zb1/sb2)}(k) \tag{33}$$

$$u_{zb2}(k) = u'_{(zb2/sa1)}(k) + u'_{(zb2/sa2)}(k) + u'_{(zb2/sb1)}(k) + u'_{(zb2/sb2)}(k) \tag{34}$$

The initial characteristic of the filter is given not only as low pass filter for avoiding control-spillover but also high pass filter for removing static signals such as the static response excited by static pressure of wind and sensor drift components. As the result, the filters defined in equation (17) and (18) are given as band pass filters which pass the range of frequency covering the control target modes. The optimum filter system which is actually used at the building is shown in Fig.9.

7. Vibration Control Performances

Table 1 shows the damping performance obtained by free vibration test. It is concluded that the performance of controlled building meets the design criterion.

Fig.10 shows the measured building responses and wind profile due to typhoon No.21 on October 1st, 2002. The “With control” and “Without control” records are obtained by switching HMDs on and off

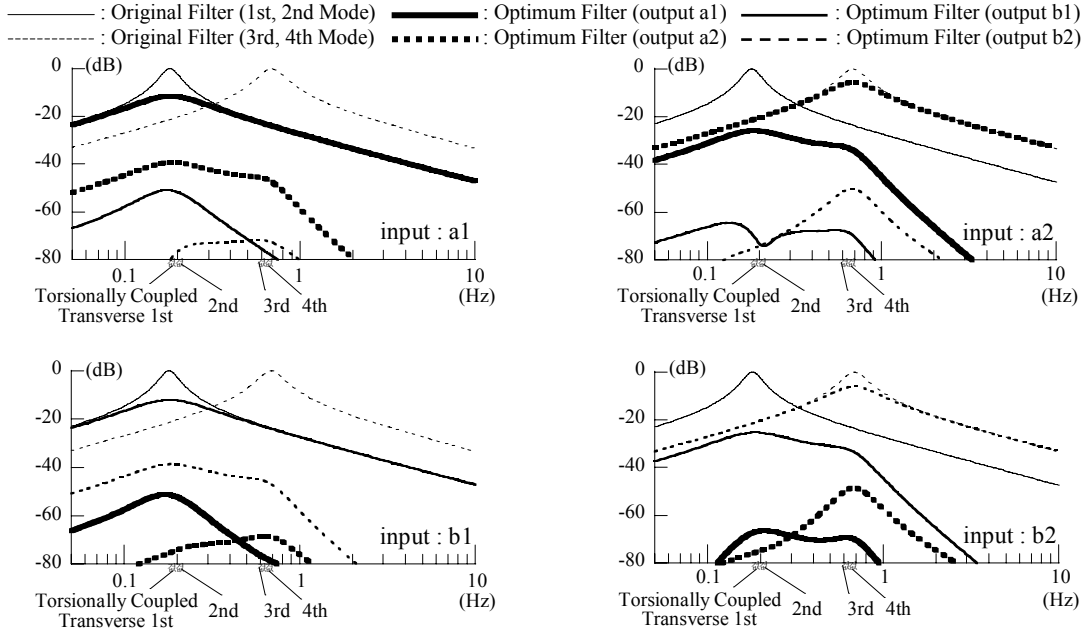

Fig. 9. Comparison between Original Filter and Optimum Filter

repeatedly with five minutes interval. The data, which have similar wind profile for "With control" and "Without control" are selected and shown in Fig.10. Note that in the case of "Without control" the TMD itself was locked using braking system. The results show that the acceleration response on the roof with control was reduced to 23% of that without control, which meets the design criterion.

8. Conclusions

1) For facilitating to manage the stroke displacement of AMD and preventing it from overshooting to input signal, we developed the method to convert the velocity controlled type of the conventional AC servomotor into the displacement controlled type with minor loops.

2) We developed the method to correct the nonlinear characteristic of TMD composed of Multi-Layer Laminated Rubber Bearing by using the compressive spring system.

3) The state equation combining above three terms and filter system is presented.

4) The method to derive the optimum filter system from the initial filter which is set in order to prevent AMD from reacting to static pressure of the wind and to avoid the control-spillover is presented.

5) We have verified the effects of a series of proposed vibration control methods from the data observed at the actual high-rise buildings.

References

1) Yoshida,K., Suzuki,T., Kageyama,M., and Nobata,A. (1991) Active Vibration Control using Dynamic Vibration Absorber Driven by Servo Motor, Colloquium on Control of Structures, JSCE, Part.B, 299-308.

2) Watanabe,T., Yoshida,K., Shimogo,T., Suzuki,T., Kageyama,M., and Nobata,A. (1992) Research on Reduced-Order Active Vibration Control for High-rise Buildings, Transactions of JSME, 58-546, PartC, 66-73

3) Suzuki,T., Kageyama,M., Nobata,A., Yoshida,O., and Inaba,S. (1996) Active Vibration Control System Installed in a High-rise Building, Eleventh World Conference on Earthquake Engineering, Paper No.19

4) Kageyama,M., Okuda,H., and Inaba,S. (1998) A Study on Stroke Saturation Control of AMD with Variable Gain, Proceedings of the Second World Conference on Structural Control Kyoto Japan, Volume1, 481-490

5) Okuda,H., and Kageyama,M. (2000) Experimental Study on the Optimum Vibration Control of AMD with Variable Gain under Stroke Constraint and with Spil-Over Prevention, Journal of Structural and Construction Engineering, AIJ, No.532, 87-94 (in Japanese).

6) A.V.Oppenheim., R.W.Schafer. (1989) Discrete-time Signal Processing, Prentice-Hall, 415-430

Table 1. Damping Performance

	Torsionally Coupled Transverse				Longitudinal
	1st Mode	2nd Mode	3rd Mode	4th Mode	1st Mode
Without Control	0.77%	0.92%	0.85%	0.83%	1.15%
With Control	12.7%	9.14%	3.17%	2.99%	3.59%

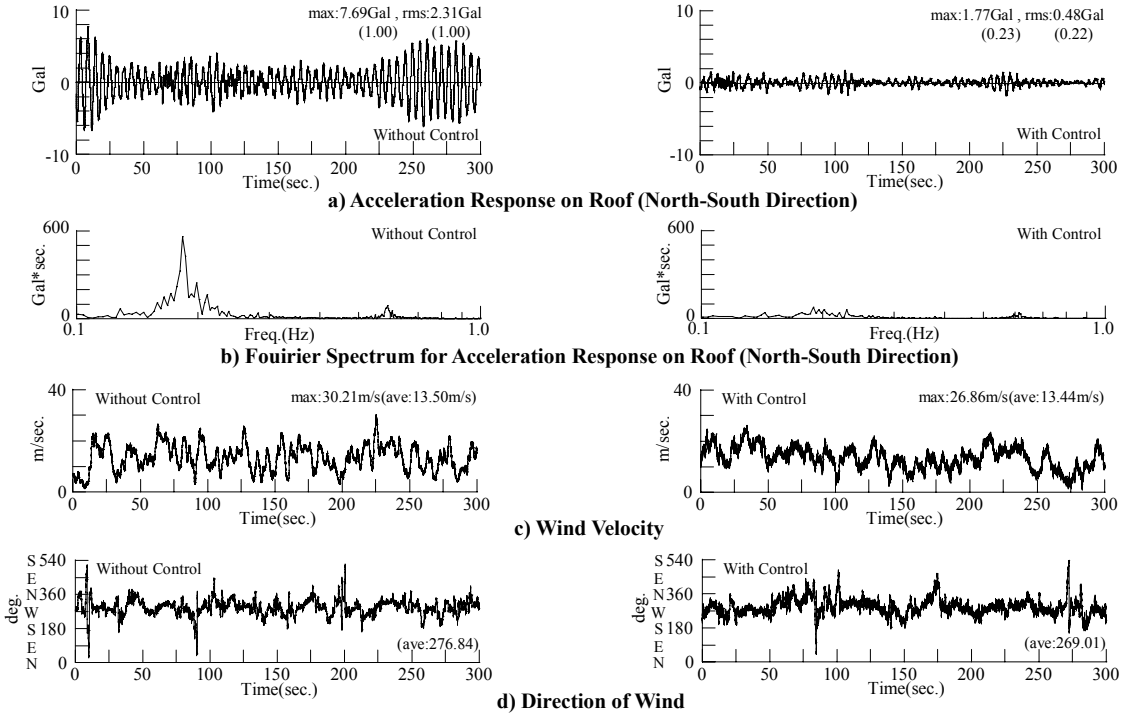

Fig. 10. Wind Observation Records (Typhoon No.21 October 1st, 2002)